Icarus **155**, 94–103 (2002)
doi:10.1006/icar.2001.6751, available online at http://www.idealibrary.com on IDEAL®

An Estimate of Eros's Porosity and Implications for Internal Structure

Sarah L. Wilkison and Mark S. Robinson

Department of Geological Sciences, Northwestern University, Evanston, Illinois 60208
E-mail: sarah@earth.nwu.edu

Peter C. Thomas and Joseph Veverka

Department of Astronomy, Cornell University, Ithaca, New York 14853

Timothy J. McCoy

Department of Mineral Sciences, National Museum of Natural History, Smithsonian Institution, Washington, DC 20560–0119

Scott L. Murchie and Louise M. Prockter

Applied Physics Laboratory, Laurel, Maryland 20723

and

Donald K. Yeomans

Jet Propulsion Laboratory, California Institute of Technology, Pasadena, California 91109

Received December 14, 2000; revised July 25, 2001

Earth-based spectral measurements and NEAR Shoemaker magnetometer, X-ray, and near-infrared spectrometer data are all consistent with Eros having a bulk composition and mineralogy similar to ordinary chondrite meteorites (OC). By comparing the bulk density of 433 Eros (2.67 ± 0.03 g/cm^3) with that of OCs (3.40 g/cm^3), we estimate the total porosity of the asteroid to be 21–33%. Macro (or structural) porosity, best estimated to be ~20%, is constrained to be between 6 and 33%. We conclude that Eros is a heavily fractured body, but we find no evidence that it was ever catastrophically disrupted and reaccumulated into a rubble pile.

Key Words: **Eros; meteorites; surfaces, asteroids; interiors.**

INTRODUCTION AND BACKGROUND

The Near Earth Asteroid Rendezvous (NEAR) Shoemaker spacecraft orbited 433 Eros from February 14, 2000 to February 12, 2001, collecting positional, image, altimetry, and spectral data through remote sensing experiments. Although NEAR Shoemaker has no instrumentation that allows for a direct measurement of the asteroid's interior structure, the density and porosity of an asteroid can give first-order information regarding the structural makeup of an asteroid. Utilizing the available density and porosity data for meteorites (Consolmagno and Britt 1998, Flynn *et al*. 1999, Wilkison and Robinson 2000) and the bulk density of Eros obtained from NEAR Shoemaker measurements (Veverka *et al*. 2000, Yeomans *et al*. 2000), we estimate a range of porosity for Eros. Additionally, we briefly review relevant asteroid formation models and how asteroids might structurally evolve over time due to impacts, and we attempt to clarify terms previously used to describe the collisionally altered parent bodies (i.e., "rubble pile"). Finally, a comparison of the formational and structural models with the estimated porosity and morphologic observations of the surface allows us to infer the gross internal structure of 433 Eros.

PARENT BODY FORMATION MODELS

Several models of applicable (for 433 Eros) parent bodies have been proposed that describe the internal structure of an asteroid before any significant structural modification (due to impacts) has occurred. In this section we briefly review these previously proposed models: the undifferentiated model, the onion shell model, the heterogeneously heated model, the metamorphosed planetesimal model, and the differentiated model (Fig. 1, column 1).

The *undifferentiated model* proposes that an asteroid is composed of primitive undifferentiated chondritic material and as such would have a solid coherent interior lacking any layering, either in composition or in alteration state (e.g., Wetherill and Chapman 1988). The classic *onion shell model* proposes that large asteroids (perhaps >50 km radius depending on thermal diffusivity) are accreted cold and heated by either external

0019-1035/02 $35.00

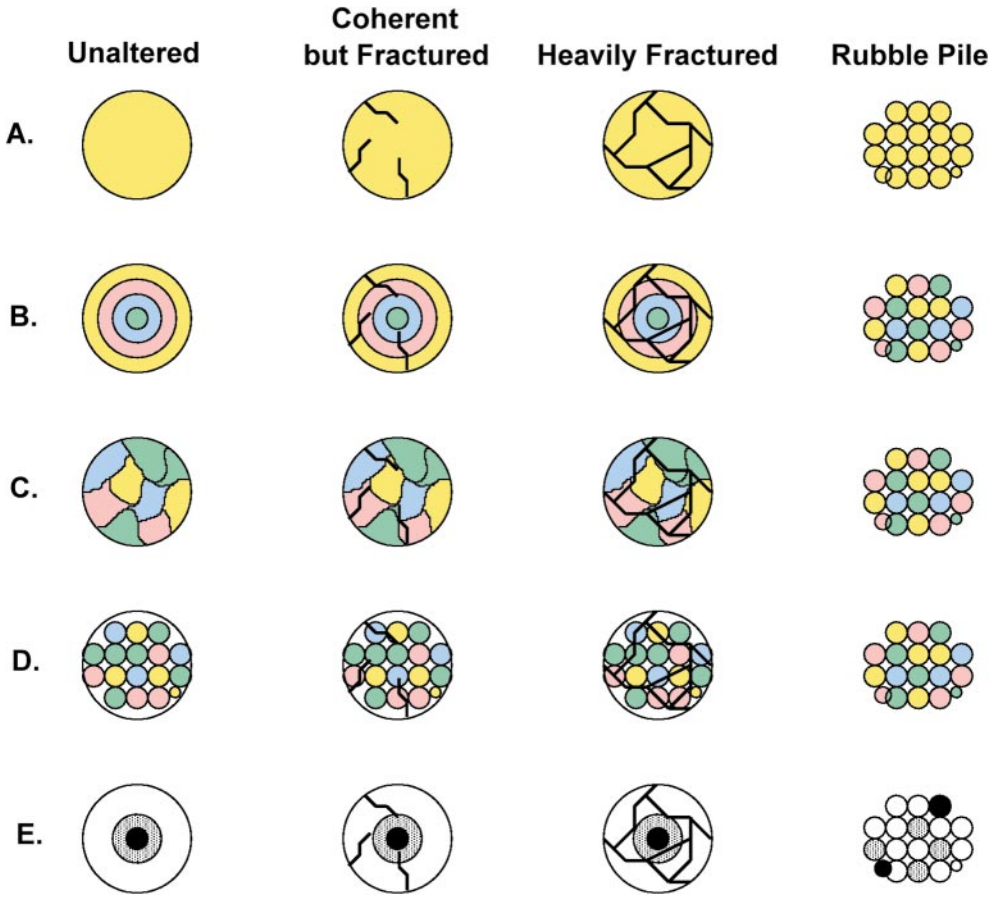

FIG. 1. Potential parent body models for 433 Eros. Colors represent different ordinary chondrite petrologic types (yellow represents petrologic type 3, red represents petrologic type 4, blue represents type 5, and green represents type 6). The five modeled asteroids could evolve with collisional modification/disruption into the three structural models (fractured but coherent body, heavily fractured, and rubble pile). Shapes and sizes of fragments are not meant to be taken literally; this is a schematic representation. (A) The undifferentiated model, after Wetherill and Chapman (1988). The asteroid is composed of undifferentiated chondritic material (in this example the material is petrologic type 3). (B) The onion shell model, after Miyamoto *et al*. (1981). The chondritic parent body exhibits successive layers of petrologic types 3 through 6. (C) The heterogeneously heated model, as described in McCoy *et al*. (1990). The chondritic body experiences heterogeneous heating throughout that results in petrologic types being dispersed randomly through the parent body. (D) The metamorphosed planetesimal model, after Scott and Rajan (1981). Small, unconsolidated chondrite planetesimals accrete into a larger parent body. (E) The differentiated model, after Wetherill and Chapman (1988).

(e.g., early luminous Sun) or internal (e.g., short-lived radionuclides ^{26}Al and/or ^{60}Fe) sources (Herndon and Herndon 1977, Minster and Allegre 1979, Pellas and Storzer 1981, Miyamoto and Fujii 1980, Miyamoto *et al*. 1981). Heating results in a concentric "onion shell" structure: internally heated bodies have cores of strongly metamorphosed type 6 material in the slowly cooling center with weakly metamorphosed type 3 material cooling rapidly near the surface (Miyamoto *et al*. 1981). McCoy *et al*. (1990) suggested a *heterogeneously heated model* (with a source of heat such as electromagnetic induction). Such a model predicts that petrologic types are randomly distributed through the parent body. A similar random distribution of petrologic types would also occur in the *metamorphosed planetesimal model*. In this model, petrologic grades are established in small planetesimals (radii less than 10 km) that are subsequently accreted into a larger body (100-km radius) near peak metamorphic temperatures for each planetesimal (Scott and Rajan 1981, Taylor *et al*. 1982; Grimm 1985). Finally, the *differentiated coherent model* proposes that the asteroid is composed of material that differentiated into a core, mantle, and crust (e.g., Wetherill and Chapman 1988). We include the differentiated model because one interpretation of Earth-based spectral data indicates that Eros may have distinct compositional units (Murchie and Pieters 1996).

COLLISIONAL EVENTS AND DISRUPTION/MODIFICATION MODELS

Collisional events are generally classified into three groups: 1. cratering, 2. fracturing or fragmentation, and 3. catastrophic fragmentation and dispersal (Davis *et al*. 1979). Cratering is defined as the excavation of debris on a large body due to a high velocity impact (Gault *et al*. 1963). Davis *et al*. (1979) define *fragmentation* or *fracturing* as the process of crushing part or all of the body. They further define *disruption* as the

process of fragmenting and dispersing a body. Davis *et al*. (1989) define *catastrophic fragmentation* as a collision in which the largest resulting piece contains 50% or less of the initial target mass. Numerical hydrocode simulations of asteroid collisions propose that most collisionally evolved bodies larger than ~1 km are highly fragmented (Asphaug and Melosh 1993, Greenberg *et al*. 1994, 1996, Love and Ahrens 1996, Melosh and Ryan 1997).

What Is a "Rubble Pile" Asteroid?

The term "rubble pile" has been used to describe several different states among a spectrum of possible asteroidal structural evolution. Discussions of the possibility that asteroids may be composed of "a loose agglomeration of material held together gravitationally" dates back at least as far as Mariner 9 studies of Phobos and Deimos (cf. Veverka *et al*. 1974). This idea was expanded upon in reports from 1977 to 1979 (Chapman 1978, Davis *et al*. 1979, Hartmann 1979) and the first use of the term "rubble pile" appeared in Davis *et al*. (1979, p. 533).

Chapman (1978) suggested that the collision rates and energies in the asteroid belt are sufficient to fragment most asteroids; during significant collisions on larger asteroids, the body may just fragment (not disperse) and form a "pile of boulders" with no internal strength (Chapman 1978). Davis *et al*. (1979) reiterate the idea that larger asteroids are most likely internally fractured but gravitationally bound "rubble piles of megaregolith." They also include some discussion of the type of target material (strong versus weak) and the outcomes that could occur with each from catastrophic and barely catastrophic impacts. Almost two decades later, Davis *et al*. (1996) made a modification of their original definition when discussing the asteroid Ida, suggesting that the few large coherent pieces of a rubble pile could be sufficiently in physical contact to transmit compressive shock waves, thus allowing such features as antipodal grooves.

Hartmann (1979) examined collisions between comparably sized bodies; the study quantified the relationship of the two bodies in terms of the mass, density, and energy of impact. One of the potential outcomes from such a collision (greater than 50 km in size) is complete disruption and subsequent reassembly into granular bodies that then lithify into breccias. This process of catastrophic dispersal (Hartmann 1979) is defined as the condition in which half the fragments are dispersed to infinity and the remaining half fall together again to make a brecciated body. Other collisional outcomes described in this study ranged from the objects rebounding from each other with little effect to complete dispersal of both asteroids.

Size and Shape of Rubble Piles

Farinella *et al*. (1982) suggested that asteroids with diameters between ~100 and 300 km could have been completely fragmented by energetic collisions and then reaccumulated into rubble piles. More recent studies based on smoothed particle hydrodynamics suggest that asteroids a few hundred meters in diameter could also be rubble piles (Love and Ahrens 1996)—a size much smaller than previous studies proposed. Homogeneous masses subjected to self-gravitational interactions are thought to take ellipsoidal equilibrium shapes (Chandrasekhar 1969, Farinella *et al*. 1981). Farinella *et al*. (1982) suggested that rubble piles sustain a shape that approximates the equilibrium figure of a fluid of similar density and spin rate. A stable shape for a body in hydrostatic or gravitational equilibrium is an ellipsoid (Chandrasekhar 1969, Farinella *et al*. 1981, Catullo *et al*. 1984, Zappala *et al*. 1984). Gravitationally reaccumulated fragments could have shapes that are approximately Maclaurin spheroids (moderate rotation rate) or Jacobi ellipsoids (fast rotation) (Farinella *et al*. 1981) depending on the largest fragment size and distribution of smaller pieces. A rubble pile consisting of a mixture of particles of very different sizes might have regions of substantially different porosities, although in general materials with poor particle size sorting have lower average porosities (Pettijohn 1957). Models of particles of randomly selected size and density can produce a wide range of offsets of the center of mass from the center of figure, and thus are not particularly diagnostic (results for Eros are discussed in the following).

Strength of Rubble Piles

Recent studies suggest that many smaller objects, including asteroids, may be held together by self-gravity, not by the tensile strength of the material. Such an asteroid would not be comparable to the strength-dominated laboratory targets from which many characteristics of asteroids have been estimated (Love and Ahrens 1996). According to models of asteroid collisions, craters can form in the "gravity scaling regime" on a target where gravity, not physical strength, controls crater size and growth (Veverka *et al*. 1974, Greenberg *et al*. 1994, 1996, Asphaug *et al*. 1996, Love and Ahrens 1996). Several large (19–33 km in diameter) craters were observed on 243 Mathilde, an asteroid that is itself only 53 km in diameter (Veverka *et al*. 1997). Stickney crater on Phobos is also thought to have formed in the gravity scaling regime (Asphaug and Melosh 1993, Love and Ahrens 1996). A target in this gravity regime must be weak or fragmented (Richardson *et al*. 1998), because a weak target dampens the propagation of shock waves (Asphaug *et al*. 1998). Harris (1996) studied the rotation periods of 107 small (less than 10-km) asteroids and observed that none of these asteroids rotate faster than the theoretical breakup limit for a gravity-dominated object, suggesting that small asteroids could be rubble piles (lack tensile strength), since solid objects could be rotating at nearly any speed (Bottke *et al*. 1998). Pravec and Harris (2000) analyzed the distribution of asteroid spin rates and sizes, concluding that asteroids larger than a few hundred meters are mostly loosely bound, gravity-dominated aggregates with negligible tensile strength. In addition, models of the tidal disruption of gravitationally bound asteroids and comets indicate that these objects may have created the abundant crater chains found on the Earth and the Moon (Bottke *et al*. 1997).

Meteoritical Evidence of Rubble Piles

Meteoritical evidence indicates that disaggregated asteroidal material may not be rare as witnessed by the relatively common meteoritic breccias. Early petrologic studies (Binns 1967, Rubin *et al*. 1983) indicated that 62% of the LL chondrites, 25% of the H chondrites, and 10% of the L chondrites are breccias. A more recent study (Benoit *et al*. 2000) suggests slightly different percentages of meteoritic breccias: 41% of the LL, 29% of the L, and 22% of the H chondrites (percentages represent an average of each of the groups, LL, L, and H). Most of the LL breccias are genomict breccias (composed of LL clasts of different petrologic types), suggesting that the LL group has had a complex collisional history that may include episodes of parent body disruption and reassembly (Rubin *et al*. 1983). Evidence supporting breakup and reassembly includes the disparity between petrologic types and metallographic cooling rates in ordinary chondrites (e.g., Taylor *et al*. 1987) and the wide range of cooling rates observed in components of various meteoritic breccias (e.g., the aubrites, Okada *et al*. 1988).

Stoffler (1982) suggested that some amount (perhaps a small fraction) of heavily shocked rock would be created during the fragmentation, disruption, and reassembly of the parent body. However, Taylor *et al*. (1987) have suggested that the breakup and reassembly of an asteroid may not produce significantly shocked material at all, depending on the sizes and velocities of the colliding bodies. Examination of meteoritic material reveals that most meteorites are unshocked or only weakly shocked (shock stage 3; Scott *et al*. 1989, Stoffler *et al*. 1991), which concurs with the Taylor *et al*. (1987) conclusion that breakup and reassembly of a parent body may not produce much heavily shocked material.

Fragmental meteoritic breccias, thought to be debris derived from different lithologies, comprise 5% of the H, 22% of the L, and 23% of the LL chondrites (Rubin *et al*. 1983). Fragmental breccias lack solar flare particle tracks and solar wind gases and have thus been assumed to have not formed within the regolith of a parent body (Rubin *et al*. 1983). However, we point out that the regolith on Eros is typically one to tens of meters in thickness (locally it may exceed 100 meters) (Barnouin-Jha *et al*. 2000, Thomas *et al*. 2001, Zuber *et al*. 2000) and we do not know the efficiency with which portions of the regolith are lithified into breccias (and are thus protected from solar flare particles and solar wind gases). Additionally, the rate of gardening on asteroidal sized bodies is unknown and thus it is not clear if material buried tens or hundreds of meters down experiences any significant solar wind exposure during its residence time in the regolith. Clearly the upper loose portion of the regolith does not survive a journey to the Earth's surface in a recognizable form.

In summary, the meteoritical evidence clearly shows that asteroids commonly produce heavily fragmented or brecciated material; however, all this material could have been produced in a regolith and there is no evidence *demanding* a rubble pile parent body.

IMPLICATIONS OF COLLISIONAL DISRUPTION/MODIFICATION

Earth-based and spacecraft imaging confirm that asteroids are heavily cratered and have thus experienced a significant degree of impact-induced fracturing. Certainly individual asteroids have suffered differing amounts of internal fracturing depending on their collisional histories. For the purpose of this study we propose three states of structural modification along the spectrum from a completely coherent to a totally disrupted and reaccreted asteroid (Fig. 1).

Coherent but fractured. The target body is mildly fractured in collisions but is still a coherent, strength-dominated body. If some fractures have passed completely through the asteroid, the fragments have *not undergone any* significant movement or rotation relative to the original structure of the asteroid. This increase in porosity (and decrease in bulk density) is an example of secondary porosity as defined by Fraser (1935).

Heavily fractured. The asteroid has been heavily fractured, possibly through several large collisions, and fragments have undergone small displacement/rotation (consistent with the Chapman (1978) and Davis *et al*. (1979) definition of a rubble pile). We infer that this structure would have more porosity that the coherent but fractured model, owing to an increase in the number of fractures and void space (macroporosity) between the displaced/rotated fragments.

Rubble pile. For the purposes of this paper we adopt the definition that a *rubble pile* is an asteroid that was reaccreted from the remnants of a disrupted parent body into a gravitationally bound granular body (i.e., consistent with descriptions in Hartmann (1979), Asphaug *et al*. (1998), and Wilson *et al*. (1999)). This definition implies little internal strength and a relatively high porosity as a result of the voids created by the reassembly of the dispersed fragments. The amount of porosity, as with terrestrial rocks, would depend upon the distribution of sizes and shapes of the particles and on the opportunities for mixing the smaller size fractions among the larger particle interstices (Pettijohn 1957).

In each of these three models the relative amount of fracturing increases, resulting in higher porosity. Two general types of porosity are discussed when describing asteroids and meteorites: microporosity and macroporosity (Consolmagno and Britt 1998, Flynn *et al*. 1999, Wilkison and Robinson 2000). Microporosity is the porosity inherent in a meteorite sample, on the same scale as the grain size, manifested as small cracks and voids. Macroporosity is the void porosity between (large) coherent pieces (such as between the pieces of a rubble pile) within an asteroid. These two generalized classifications of porosity represent endmembers; a continuum of porosity probably exists, but because of the lack of asteroid ground truth and for ease of discussion, we use these terms for clarity.

Tentative porosity ranges can be assigned to each of the three asteroid structural models from terrestrial and lunar analogs

TABLE I
Porosities of Rocks

Sample	Porosity (%)	Reference
	Lunar samples	
Breccia	17.4	Horai and Winkler (1976)
Breccia	14.1	Horai and Winkler (1976)
Breccia	24	Horai and Winkler (1980)
Breccia	4.9	Fujii and Osako (1973)
Welded microbreccias	18.4–43.9	Chao *et al.* (1971)
Lunar regolith	46	Carrier *et al.* (1991)
	Terrestrial impact samples	
Coconino sandstone	24	Ahrens and Gregson (1964)
Lappajarvi breccias	up to 20	Kukkonen *et al.* (1992)
"Shocked sandstone"	up to 23	Short (1966)
	Common rocks	
Unconsolidated sand	38.7–44.8	Schopper (1982)
Nonindurated sand	33.8–51.3	c.f. Davis (1969)
Gravel	63.4	Cohen (1965)
Bunter sandstone	5.8–30.8	Schopper (1982)
Welded tuff	14.1	Keller (1960)

(Table I). OC meteorites *generally* fall within the bulk porosity range 0–15% (Consolmagno and Britt 1998, Flynn *et al.* 1999) (outliers from the 0–15% porosity range are discussed in more detail below). Ordinary chondrite (OC) meteorite samples do not exhibit abundant fractures or other post-formation modification that would affect their bulk porosity (their porosity is all microporosity). Thus we propose a range of 0–15% for the *coherent but fractured* asteroid model.

Microporosity values for lunar breccias generally range from 5 to 24% measured from small samples, and porosities from terrestrial impact sites range from 20 to 24% (Table I). Ahrens and Gregson (1964) shocked Coconino sandstone in the laboratory and measured the porosity at 24%. A detailed study of the terrestrial Lappajarvi breccias investigated both micro- and macroporosity of impact rocks (Kukkonen *et al.* 1992). Analysis of materials from the Lappajarvi drill core and resistivity logs found that "the apparent and rock sample porosity profiles are remarkably similar in their overall shape, which indicates that a considerable part of the effective porosity of rocks is due to small-scale pores and vesicles. The apparent porosities are slightly higher than the core sample porosities as a result of fractures" (Kukkonen *et al.* 1992). This conclusion indicates that the porosity of the drill core (up to 20%) itself is representative of the whole rock unit (impact site). Short (1966) discovered that shock-lithified sand formed coherent masses ("shocked sandstone") during cratering explosions at the Nevada Test Site; these masses resembled shocked sandstones found at meteorite craters (such as Wabar, Saudi Arabia). The porosity of the shock-lithified sand masses ranges up to 23% (Short 1966). These impact samples (lunar and terrestrial) suggest that the *heavily fractured* asteroid model proposed above could have total porosity ranging from 15 to 30%.

Finding a terrestrial or lunar analog for a *rubble pile* asteroid is admittedly problematic. Unconsolidated terrestrial sediments can have porosities of 20–50% or even over 60% (Table I). The particle size sorting is critical in determining the porosity, and for very fine terrestrial sediments, particle shapes, compaction, and mechanism of deposition affect porosity greatly. The best terrestrial analogs for rubble pile structures may be fresh rockfall or landslide deposits and mine dumps, as they would have minimal effects of fluvial addition or removal of fines that can change porosity. Measurement of such porosities, however, is notoriously difficult, and the analogy may not avoid the effects of 100- 1000-fold difference in compressive stresses between terrestrial rubble pile deposits and small asteroids. Nonetheless, the analogies and geometry of packing fragments suggest that rubble piles could have porosities well in excess of 30%. Another potential analog for a rubble pile asteroid is the lunar regolith, which is composed of unconsolidated lithic fragments. An estimate of lunar regolith porosity in situ (for the top 0–60 cm) is $46 \pm 2\%$ (Carrier *et al.* 1991). Finally, modeling of the collisional breakup and gravitational assembly process predict porosities of $\sim$40% for asteroids that have undergone breakup and reassembly (Wilson *et al.* 1999). However, subsequent settling and relithification may lower this value to the range of $\sim$30%. We adopt $>30\%$ as the porosity for a rubble pile (as defined in this manuscript). Clearly these porosity boundaries are rough and will remain so until direct measures (such as seismic data) of a statistically significant population of asteroid interiors are obtained.

Implications for the Parent Body Models

We illustrate the evolution of the parent body models (undifferentiated coherent, onion shell, heterogeneously heated, metamorphosed planetesimal, and differentiated coherent) through time (Fig. 1, columns 2–4); each model and its resulting characteristics are classified according to the three modification/disruption models proposed (coherent but fractured, heavily fractured, and rubble pile). As demonstrated by Fig. 1, many of the resulting structural models are not easily distinguishable from each other. Even existing remote sensing data may not distinguish between the resulting structural models, let alone allow us to determine the unaltered parent body structure. We include this illustration to emphasize the importance of using the porosity estimate, along with existing remote sensing data, to infer the internal structure of an asteroid.

DISCUSSION

Composition

Telescopic spectral data indicated that Eros might be compositionally heterogeneous on a hemispheric level (Murchie and Pieters 1996). However, color and spectral measurements of Eros from the NEAR Shoemaker Multispectral Imager (MSI) and the near-infrared spectrometer (NIS) did not confirm this

result (Murchie *et al*. 2000, Murchie *et al*. 2001, Bell *et al*. 2001). NEAR Shoemaker X-ray/gamma-ray Spectrometer (XGRS) data indicate that Eros has an elemental composition (Fe, Mg, Ca, and Al, ratioed to Si) consistent with undifferentiated ordinary chondritic (H, L, or LL) meteoritic material (Trombka *et al*. 2000). NEAR Shoemaker NIS spectra and MSI color results are also consistent with an ordinary chondrite composition (Veverka *et al*. 2000, Murchie *et al*. 2001, Bell *et al*. 2001). Additionally, NEAR Shoemaker magnetometer results also show Eros to have a composition consistent with LL OCs (Acuna *et al*. 2000). Finally, the fact that Eros's center of mass and center of figure are nearly coincident (as described in the next section) rule out large inhomogeneities in its internal density, which would be expected if Eros exhibited large internal compositional units (Thomas *et al*. 2001). These results allow us to compare the calculated density for Eros to that of OC meteorites.

Porosity

Consolmagno and Britt (1998) measured the microporosities of 15 ordinary chondrites and found them to range from 0 to 15%. Another study (Flynn *et al*. 1999) reports OC microporosities from 0 to 23% ($n = 27$). Unfortunately, the total number of well-documented OC microporosities is 42 (Fig. 2). The median porosity value of ordinary chondrities in each study was 6%, the averages were 6.5% and 6.4%, (respectively), and the standard deviations were 4.1% and 6.8% (respectively). We note that Flynn *et al*. (1999) measured the porosities of two pieces of Bjurbole to be 20% and 23% porosity. The Bjurbole samples are extremely friable to the point that they crumble with handling (Flynn *et al*. 1999). Clearly this texture is rare among OCs, and the origin of this texture is not understood. Perhaps Bjurbole is not representative of the original asteroid's porosity but may be more similar to a regolith porosity.

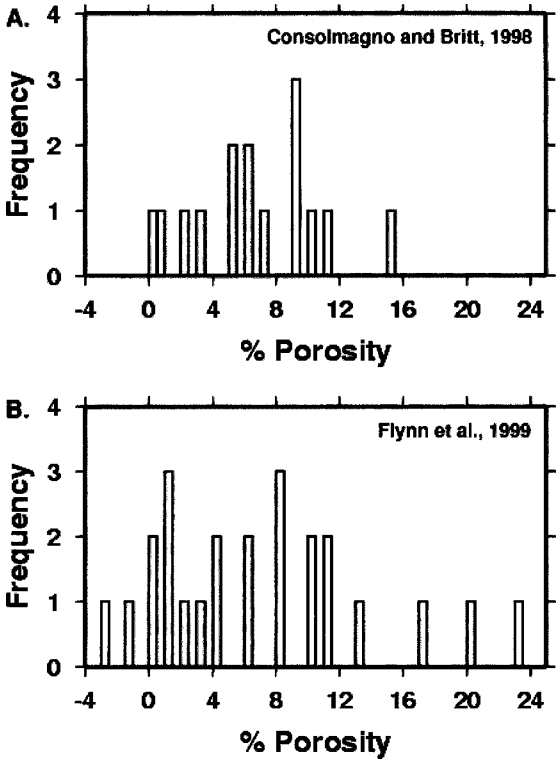

FIG. 2. Histograms of ordinary chondrite porosities from two datasets. Both studies overlap in the 0–15% range of porosity; both studies have median porosities of 6%. (A) From Consolmagno and Britt (1998). (B) From Flynn *et al*. (1999).

TABLE II
Estimations of Eros's Porosity

Bulk density (OC) (g/cm^3)	*3.40*	*3.40*	*3.40*	*3.40*	*3.40*
Microporosity (OC)	0%	0%	15%	15%	6%
Grain density (OC) (g/cm^3)	*3.40*	*3.40*	*4.00*	*4.00*	*3.62*
Total porosity (Eros)	*21%*	*21%*	*33%*	*33%*	*26%*
Microporosity (Eros)	0%	15%	0%	15%	6%
Macroporosity (Eros)	*21%*	*6%*	*33%*	*18%*	*20%*

Notes. Numbers in italics represent calculations; numbers not italicized represent assumptions. Read down each column. Each column illustrates an estimation of Eros's porosity starting with the average bulk density of OCs (row 1). Microporosities of the meteorite are assumed to be in the range 0–15% and the median is 6% porosity (row 2). Row 3 shows the calculated grain densities based on the previous assumptions (rows 1 and 2). The grain density is then compared with Eros's bulk density of 2.67 g/cm^3, resulting in the estimate of the total porosity of Eros (row 4). More assumptions are made about the microporosity of Eros (row 5), which leads to the calculation of Eros's macroporosity (row 6). Note that we have chosen to use the average bulk density (3.40 g/cm^3) of OCs in this estimation. If there were more porosity and density data available, a more rigorous approach would be to estimate the porosity of Eros using varying bulk densities and microporosities of OCs and varying microporosities of Eros.

We choose a more conservative measure of OC porosity, 0–15%, a range at which both studies (Consolmagno and Britt 1998, Flynn *et al*. 1999) overlap (see Fig. 2). Table II illustrates our estimates of the porosity of Eros using varying microporosities of OCs and varying microporosities of Eros. Using the range of porosity (0–15%) for OCs, the average bulk density of OCs, 3.40 g/cm^3 (Wilkison and Robinson 2000), and the bulk density of Eros, 2.67 ± 0.03 g/cm^3 (Veverka *et al*. 2000, Yeomans *et al*. 2000), we estimate the total porosity of Eros to be 21–33% (Wilkison and Robinson 2000). We infer that Eros's macroporosity may be as high as 33% (0% microporosity, 33% total porosity) but must be greater than 6% (15% microporosity, 21% total porosity) (Table II). Using the median value of 6% porosity of OCs, the average bulk density of OCs, and the bulk density of Eros, we estimate the total porosity of Eros to be ∼26%: removing 6% microporosity from the asteroid would leave a macro- (or structural) porosity of ∼20% (Table II).

Modeling of the collisional breakup and gravitational assembly process predict porosities of ∼40% for asteroids that have undergone breakup and reassembly (Wilson *et al*. 1999). Variations in porosity within an object might be detected by a difference in the object's gravity field from that of a completely homogeneous object. Assemblage of a rubble pile having a range of fragment sizes should exhibit variations in porosity, and hence local

density, within the object. However, NEAR Shoemaker gravity data indicate that Eros has a nearly uniform density (Yeomans *et al*. 2000, Zuber *et al*. 2000).

The tracking of the NEAR Shoemaker spacecraft has been accurate to well under 100 m (Yeomans *et al*. 2000), and this has allowed accurate comparisons of the center of mass with the center of figure. The center of mass offset from the center of figure for Eros is ∼52 m, or about 0.6% of the object's mean radius (Thomas *et al*. 2001). This offset can be simulated by a layer at high latitudes of approximately 250 m of material 30% underdense relative to the rest of the asteroid, or by many other combinations of thickness and relative density. This example of a modestly different density layer only a few percent of the mean radius illustrates the generally homogeneous nature of Eros and is consistent with a layer of regolith on the surface.

Morphology

Structural continuity of an asteroid is suggested by the presence of grooves and ridges (Veverka *et al*. 1974, Thomas *et al*. 1979, 1992, 1994). Grooves are considered to be expressions of structural features—especially when such features are in preferred directions and orientations (Veverka *et al*. 1994). Based on observations of Phobos, two theories have been proposed as explanations for pitted grooves: either they indicate the collapse of loose material into fractures or they indicate the expulsion of material from fractures (Thomas *et al*. 1979, Horstmann and Melosh 1989). Gaspra has grooves that fall into two groups of orientations; the pattern of grooves and ridges observed indicates a global fabric that implies that Gaspra is a single, coherent object (Thomas *et al*. 1994). Sullivan *et al*. (1996) suggest that the

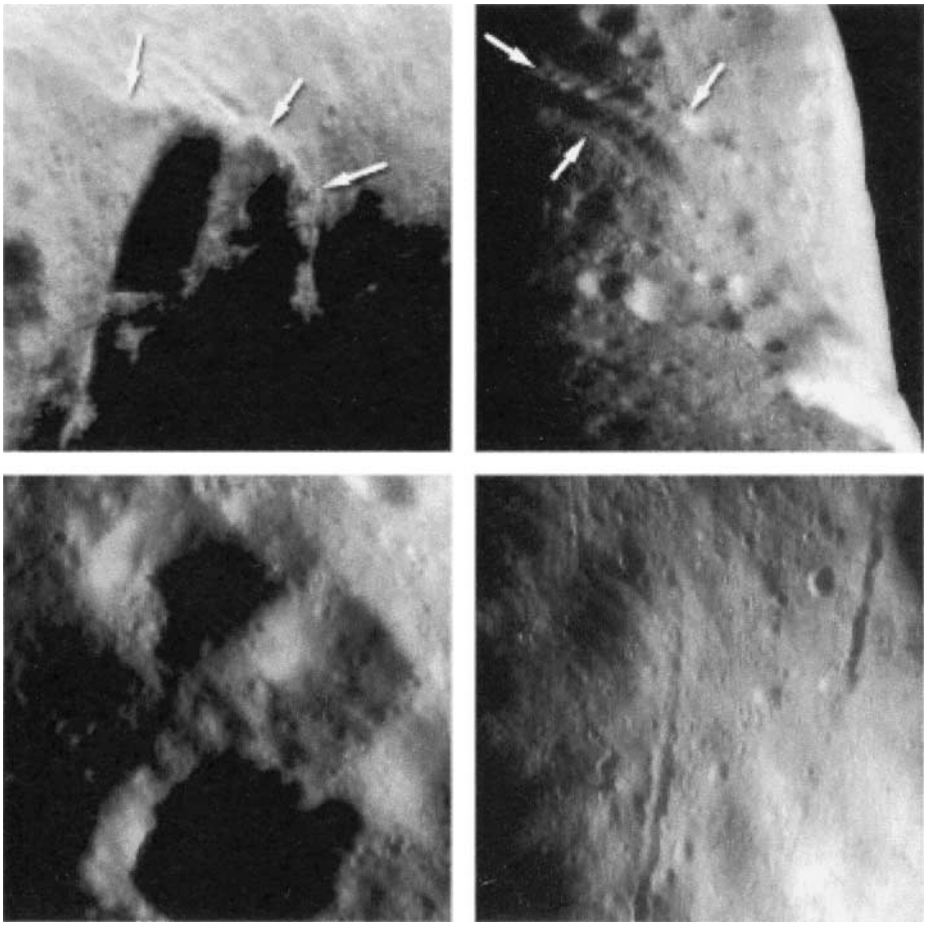

FIG. 3. Four examples of morphologic features found on Eros that suggest the asteroid has a global internal strength. (Upper left) Rahe Dorsum is a ridge with over 300 m (Cheng *et al*. 2001) of relief and it stretches for ∼15 km in length (Veverka *et al*. 2000). The steepest face of the ridge has a slope of greater than 60°, indicating that is formed in competent material (well above the angle of repose of loose material, Cheng *et al*. 2001) (MET 131968549–131969115B). (Upper right) Prominent set of ridges "twist" (Veverka *et al*. 2000) consistent with an extensional stress environment in a competent material (MET 129525607–129525697). (Lower left) Square craters are known to form as a result of impact into a solid rock with a preexisting fracture pattern (Shoemaker 1963) such as those found on the western end (∼320° W) of Eros (MET 132151511, 132151569). (Lower right) Much of Eros is patterned in a complex series of grooves and "fabric" interpreted to indicate a competent lithology beneath the regolith (Veverka *et al*. 2000). In this mosaic two longitudinal grooves exhibit aligned pits similar to those found on Phobos (MET 135343994–135345734).

grooves of Ida are internal fractures expressed in a surface layer of less coherent materials.

Structural features such as lineations have been observed on Eros (Veverka *et al*. 2000, Prockter *et al*. 2000, 2001 and include sinuous and linear depressions, topographic ridges, and alignment of sections of the terminator (Fig. 3) (Veverka *et al*. 2000). Evidence of preexisting fabric in smaller craters, which exhibit elongation in the direction of intersecting or adjacent lineaments, has also been observed (Prockter *et al*. 2000, 2001).

A prominent ridge system (Fig. 3; Rahe Dorsum) spans the northern hemisphere and geometrically defines a planar slice through the asteroid (Veverka *et al*. 2000, Prockter *et al*. 2001). This ridge crosscuts structures such as Himeros, indicating that it was created after Eros retained its current shape (Veverka *et al*. 2000). Rahe Dorsum has slopes well above the angle of repose (Cheng *et al*. 2001) and is continuous across more than a third of an Eros circumference, and it exhibits a morphology consistent with a compressive fault plane through a consolidated or coherent material. A set of parallel ridges on the opposite side of Eros, informally called the "twist," constitutes a second set of prominent ridges. A global extent of the asteroid's fabric is suggested by the alignment of Rahe Dorsum and the twist. These two features lie in one plane (within 400 m over a 15-km length), and Rahe Dorsum by itself defines the same planar feature. Because of their different morphology, these surface features probably represent different responses of a global fabric to impact erosion (the twist?) or stresses (Rahe Dorsum?), and they may have formed at different times. Veverka *et al*. (2000) suggested that the large variation in directions and patterns of the shorter lineations indicate that they were formed in many different events. Grooves crosscut the oldest craters on Eros, but younger craters crosscut some of the grooves (Veverka *et al*. 2000). These features all indicate that Eros possesses structural continuity and internal strength.

Observations of morphological features on Eros such as regions of high slopes, continuous grooves, steep continuous ridges, and fault planes suggest that the asteroid possesses global mechanical strength and is not strictly a gravitationally bound object (Thomas *et al*. 2001, Zuber *et al*. 2000). These structures indicate that Eros, unlike rubble pile models, possesses significant internal strength.

CONCLUSIONS

All available bulk compositional estimates for Eros suggest that it is an OC type body, thus allowing us to estimate its total porosity (21–33%) from measures of meteoritic material and Eros's bulk density. Using the median value of microporosity for the meteorites, we estimate that Eros has a macroporosity of 20%. This value is consistent with impact breccias found on the Earth and Moon, indicating that Eros has suffered a high degree of impact-induced fracturing (eliminating the *coherent yet fractured* model). Is Eros a *heavily fractured* or *rubble pile* asteroid? The remaining circumstantial evidence leads us to believe that Eros is not a rubble pile (as defined here). First, the range of estimates for Eros's macroporosity, while not conclusive, are lower than rubble pile models would suggest. Modeling of the collisional breakup and gravitational assembly process predicts porosities of ∼40% for asteroids that have undergone breakup and reassembly (Wilson *et al*. 1999), and rubble pile analogs such as the lunar regolith and unconsolidated terrestrial sediments have porosities greater than 40% (Table I). Second, the apparent homogeneity in mass distribution within Eros (Thomas *et al*. 2001, Yeomans *et al*. 2000, Zuber *et al*. 2000) suggests an implausible continuity of density for a rubble pile. Finally, structural features on its surface show that it has a significant degree of internal strength. Thus we conclude that Eros is a *heavily fractured* asteroid.

REFERENCES

Acuna, M., C. Russell, T. Mulligan, B. Anderson, L. Zanetti, D. Lohr, J. Hayes, B. Toth, and N. Omidi 2000. Magnetic field observations at 433 Eros: NEAR results. *Eos* (Fall Suppl.) 805.

Ahrens, T., and V. Gregson 1964. Shock compression of crustal rocks: Data for quartz, calcite, and plagioclase rocks. *J. Geophys. Res.* **69**, 4839–4874.

Asphaug, E., and H. J. Melosh 1993. The Stickney impact of Phobos: A dynamical model. *Icarus* **101**, 144–164.

Asphaug, E., J. M. Moore, D. Morrison, W. Benz, M. C. Nolan, and R. J. Sullivan 1996. Mechanical and geological effects of impact cratering on Ida. *Icarus* **120**, 158–184.

Asphaug, E., S. J. Ostro, R. S. Hudson, D. J. Scheeres, and W. Benz 1998. Disruption of kilometre-sized asteroids by energetic collisions. *Nature* **393**, 437–440.

Barnouin-Jha, O., A. F. Cheng, L. M. Prockter, S. Murchie, M. Zuber, D. Smith, G. Neumann, J. Garvin, M. Robinson, J. Veverka, and P. Thomas 2000. Characterizing the regolith of 433 Eros from laser altimeter and imaging. *Eos* (Fall), 805.

Bell, J. F. III, N. I. Izenberg, P. G. Lucey, B. E. Clark, C. Peterson, M. J. Gaffey, J. Joseph, B. Carcich, A. Harch, M. E. Bell, J. Warren, P. D. Martin, L. A. McFadden, D. Wellnitz, S. Murchie, M. Winter, J. Veverka, P. Thomas, M. S. Robinson, M. Malin, and A. Cheng 2002. Near-IR reflectance spectroscopy of 433 Eros from the NIS instrument on the NEAR mission. 1. Low phase angle observations. *Icarus* **155**, 119–144.

Benoit, P., D. Sears, J. Akridge, P. Bland, F. Berry, and C. Pillinger 2000. The non-trivial problem of meteorite pairing. *Meteor. Planet. Sci.* **35**, 393–417.

Binns, R. A. 1967. Structure and evolution of non-carbonaceous chondritic meteorites. *Earth Planet. Sci. Lett.* **2**, 23–28.

Bottke, W. F., D. C. Richardson, and S. G. Love 1997. Can tidal disruption of asteroids make crater chains on the Earth and Moon? *Icarus* **126**, 470–474.

Bottke, W. F., D. C. Richardson, and S. G. Love 1998. Production of Tunguska-sized bodies by Earth's tidal forces. *Planet. Space Sci.* **46**, 311–322.

Carrier, W. D., G. R. Olhoeft, and W. Mendell 1991. Physical properties of the lunar surface. In *Lunar Sourcebook* (G. H. Heiken, D. T. Vaniman, and B. M. French, Eds.), pp. 475–594. Cambridge Univ. Press, Cambridge, UK.

Catullo, V., V. Zappala, P. Farinella, and P. Paolicchi 1984. Analysis of the shape distribution of asteroids. *Astron. Astrophys.* **138**, 464–468.

Chandrasekhar, S. 1969. *Ellipsoidal Figures of Equilibrium*. Yale Univ. Press, New Haven, CT.

Chao, E. C. T., J. A. Boreman, and G. A. Desborough 1971. The petrology of unshocked and shocked Apollo 11 and Apollo 12 microbreccias. *Proc. Second Lunar Sci. Conf.* **1**, 797–816.

Chapman, C. R. 1978. Asteroid collisions, craters, regoliths, and lifetimes. *NASA Conf. Publ.* **2053**, 145–160.

Cheng, A. F., O. Barnouin-Jha, L. Prockter, M. T. Zuber, G. Neumann, D. E. Smith, J. Garvin, M. S. Robinson, J. Veverka, and P. C. Thomas 2002. Small scale topography of 433 Eros from laser altimetry and imaging. *Icarus* **155**, 51–74.

Cohen, P. 1965. Water resources of the Humboldt River Valley near Winnemucca, Nevada. U.S. Geol. Surv. Water-Supply Pap. 1795.

Consolmagno, G. J. and D. T. Britt 1998. The density and porosity of meteorites from the Vatican collection. *Meteor. Planet. Sci.* **33**, 1231–1241.

Davis, D. R., C. R. Chapman, R. Greenberg, S. J. Weidenschilling, and A. W. Harris 1979. Collisional evolution of asteroids: Populations, rotations, and velocities. In *Asteroids* (T. Gehrels, Ed.), pp. 528–557. Univ. of Arizona Press, Tucson.

Davis, D. R., S. J. Weidenschilling, P. Farinella, P. Paolicchi, and R. P. Binzel 1989. Asteroid collisional history: Effects on sizes and spins. In *Asteroids II* (R. Binzel, T. Gehrels, and M. S. Matthews, Eds.), pp. 805–826. Univ. of Arizona Press, Tucson.

Davis, D. R., C. R. Chapman, D. D. Durda, P. Farinella, and F. Marzari 1996. The formation and collisional/dynamical evolution of the Ida/Dactyl system as part of the Koronis family. *Icarus* **120**, 220–230.

Davis, S. N. 1969, Porosity and permeability of natural materials. In *Flow Through Porous Media* (R. J. M. De Wiest, Ed.), pp. 54–86. Academic Press, New York.

Farinella, P., P. Paolicchi, E. F. Tedesco, and V. Zappala 1981. Triaxial equilibrium ellipsoids among the asteroids? *Icarus* **46**, 114–123.

Farinella, P., P. Paolicchi, and V. Zappala 1982. The asteroids as outcomes of catastrophic collisions. *Icarus* **52**, 409–433.

Flynn, G. J., L. B. Moore, and W. Klöck 1999. Density and porosity of stone meteorites: Implications for the density, porosity, cratering, and collisional disruption of asteroids. *Icarus* **142**, 97–105.

Fraser, H. J. 1935. Experimental study of the porosity and permeability of clastic sediments. *J. Geol.* **43**, 910–1010.

Fujii, N., and M. Osako 1973. Thermal diffusivity of lunar rocks under atmospheric and vacuum conditions. *Earth Planet. Sci. Lett.* **18**, 65–71.

Gault, D., E. Shoemaker, and H. Moore 1963. Spray ejected from the lunar surface of meteoroid impact. NASA TND 1767, p. 39.

Greenberg, R., M. C. Nolan, W. F. Bottke, R. A. Kolvoord, and J. Veverka 1994. Collisional history of Gaspra. *Icarus* **107**, 84–97.

Greenberg, R., W. F. Bottke, M. Nolan, P. Geissler, J.-M. Petit, D. D. Durda, E. Asphaug, and J. Head 1996. Collisional and dynamical history of Ida. *Icarus* **120**, 106–118.

Grimm, R. E. 1985. Penecontemporaneous metamorphism, fragmentation, and reassembly of ordinary chondrite parent bodies. *J. Geophys. Res.* **90**, 2022–2028.

Harris, A. W. 1996. The rotation rates of very small asteroids: Evidence for rubble pile structure. *Lunar Planet. Sci.* **27**, 493–494.

Hartmann, W. K. 1979. A special class of planetary collisions: Theory and evidence. *Proc. Lunar Planet. Sci. Conf.* **10**, 1897–1916.

Herndon, J. M., and M. A. Herndon 1977. Aluminum-26 as a planetoid heat source in the early Solar System. *Meteoritics* **12**, 459–465.

Horai, K., and J. L. Winkler 1976. Thermal diffusivity of four Apollo 17 rock samples. *Proc. Lunar Sci. Conf.* **7**, 3183–3204.

Horai, K., and J. L. Winkler 1980. Thermal diffusivity of two Apollo 11 samples, 10020,44 and 10065,23: Effect of petrofabrics on the thermal conductivity of porous lunar rocks under vacuum. *Proc. Lunar Planet. Sci. Conf.* **11**, 1777–1788.

Horstmann, K., and J. Melosh 1989. Drainage pits in cohesionless materials: Implications for the surface of Phobos. *J. Geophys. Res.* **94**, 12433–12441.

Keller, G. 1960. Physical properties of tuffs of the Oak Spring Formation Nevada. U.S. Geol. Surv. Prof. Pap. 400-B, pp. 396–400.

Kukkonen, I. T., L. Kivekas, and M. Paananen 1992. Physical properties of karnaite (impact melt), suevite and impact breccia in the Lappajarvi meteorite crater, Finland. *Tectonophysics* **216**, 111–122.

Love, S. G., and T. J. Ahrens 1996. Catastrophic impacts on gravity dominated asteroids. *Icarus* **124**, 141–155.

McCoy, T. J., G. J. Taylor, E. R. D. Scott, and K. Keil 1990. Metallographic cooling rates correlated with petrologic type in LL3.0-4 chondrites: Implications for parent body structures. *Lunar Planet. Sci. Conf.* **21**, 749–750 (abstract).

Melosh, H. J., and E. V. Ryan 1997. Asteroids: Shattered but not dispersed. *Icarus* **129**, 562–564.

Minster, J. F., and C. Allegre 1979. ^{87}Rb-^{87}Sr chronology of H chondrites: Constraint and speculations on the early evolution of their parent body. *Earth Planet. Sci. Lett.* **42**, 333–347.

Miyamoto, M., and N. Fujii 1980. A model of the ordinary chondrite parent body: An external heating model. *Mem. NIPR* **17**, 291–298.

Miyamoto, M., N. Fujii, and H. Takeda 1981. Ordinary chondrite parent body: An internal heating model. *Proc. Lunar Planet. Sci. Conf.* **12B**, 1145–1152.

Murchie, S. L., and C. M. Pieters 1996. Spectral properties and rotational spectral heterogeneity of 433 Eros. *J. Geophys. Res.* **101**, 2201–2214.

Murchie, S., J. Veverka, M. Robinson, P. Thomas, J. F. Bell, N. Izenberg, C. Chapman, A. Harch, M. Bell, B. Carcich, A. Cheng, B. Clark, D. Domingue, D. Dunham, R. Farquhar, M. Gaffey, E. Hawkins, J. Joseph, R. Kirk, H. Li, P. Lucey, M. Malin, L. McFadden, W. Merline, J. Miller, W. Owen, C. Peterson, L. Prockter, J. Warren, D. Wellnitz, B. Williams, D. Yeomans, and B. Bussey 2000. Imaging and infrared spectroscopy results from NEAR MSI and NIS at Eros. *Eos* (Fall Suppl.) 803.

Murchie, S., M. S. Robinson, B. Clark, H. Li, P. C. Thomas, J. Joseph, B. Bussey, D. Domingue, J. Veverka, N. Izenberg, and C. Chapman 2002. Color variations on Eros from NEAR Multispectral imaging. *Icarus* **155**, 145–168.

Okada, A., K. Keil, J. G. Taylor, and H. E. Newsom 1988. Igneous history of the aubrite parent asteroid: Evidence from the Norton County enstatite achondrite. *Meteoritics* **23**, 59–74.

Pellas, P., and D. Storzer 1981. ^{244}Pu fission track thermometry and its application to stony meteorites. *Proc. R. Soc. London* **A374**, 253–270.

Pettijohn, F. J. 1957. *Sedimentary Rocks*. Harper and Row, New York.

Pravec, P., and A. W. Harris 2000. Fast and slow rotation of asteroids. *Icarus* **148**, 12–20.

Prockter, L., P. Thomas, J. Veverka, B. Bussey, M. S. Robinson, S. Murchie, D. Domingue, and the NEAR MSI-NIS Team. 2000. Structural features on Eros. *Eos* (Spring Suppl.) 286.

Prockter, L. M., P. C. Thomas, M. S. Robinson, J. Joseph, A. Milne, B. Bussey, J. Veverka, and A. F. Cheng 2002. Surface expressions of structural features on Eros. *Icarus* **155**, 75–93.

Richardson, D. C., W. F. Bottke, and S. G. Love 1998. Tidal distortion and disruption of Earth-crossing asteroids. *Icarus* **134**, 47–76.

Rubin, A. E., A. Rehfeldt, E. Peterson, K. Keil, and E. Jarosewich 1983. Fragmental breccias and the collisional evolution of ordinary chondrite parent bodies. *Meteoritics* **18**, 179–196.

Schopper, J. R. 1982. Porosity and permeability. In *Landolt-Bornstein-Numerical Data and Functional Relationships in Science and Technology*, New Series, Group V: Geophysics and Space Research, Vol. 1, Sub-vol. A. (O. Madelung, Ed.), p. 373. Springer-Verlag, Berlin.

Scott, E. R. D., and R. S. Rajan 1981. Metallic minerals, thermal histories, and parent bodies of some xenolithic, ordinary chondrite meteorites. *Geochim. Cosmochim. Acta* **45**, 53–67.

Scott, E. R. D., G. J. Taylor, H. E. Newsom, F. Herbert, M. Zolensky, and J. F. Kerridge 1989. Chemical, thermal and impact processing of asteroids. In *Asteroids II* (R. Binzel, T. Gehrels, and M. S. Matthews, Eds.,) pp. 701–739. Univ. of Arizona Press, Tucson.

Shoemaker, E. M. 1963. Impact mechanics at Meteor Crater, Arizona. In *The Solar System, Vol.* 4., *The Moon, Meteorites, and Comets* (B. M. Middlehurst and G. P. Kuiper, Eds.), pp. 301–336. Univ. of Chicago Press, Chicago.

Short, N. M. 1966. Shock-lithification of unconsolidated rock materials. *Science* **154**, 382–384.

Stöffler, D. 1982. Terrestrial impact breccias. In *Lunar Breccias and Soils and Their Meteoritic Analogs* (G. J. Taylor and L. L. Wilkening, Eds.) pp. 139–146. LPI Tech. Rep. 82-02. Lunar and Planetary Institute, Houston.

Stöffler, D., K. Keil, and E. R. D. Scott 1991. Shock metamorphism of ordinary chondrites. *Geochim. Cosmo. Acta.* **55**, 3845–3867.

Sullivan, R., R. Greeley, R. Pappalardo, E. Asphaug, J. M. Moore, D. Morrison, M. Belton, M. Carr, C. Chapman, P. Geissler, R. Greenberg, J. Granahan, J. Head, R. Kirk, A. McEwen, P. Lee, P. Thomas, and J. Veverka 1996. Geology of 243 Ida. *Icarus* **120**, 119–139.

Taylor, G. J., E. R. D. Scott, A. E. Rubin, P. Maggiore, and K. Keil 1982. Structure and fragmentation of the parent asteroids of ordinary chondrites. *Lunar Planet. Sci.* **13**, 799–800 (Abstract).

Taylor, G. J., P. Maggiore, E. R. D. Scott, A. E. Rubin, and K. Keil 1987. Original structures, and fragmentation and reassembly histories of asteroids: Evidence from meteorites. *Icarus* **69**, 1–13.

Thomas, P., J. Veverka, A. Bloom, and T. C. Duxbury 1979. Grooves on Phobos: Their distribution, morphology, and possible origins. *J. Geophys. Res.* **84**, 8457–8477.

Thomas, P., J. Veverka, J. Bell, J. Lunine, and D. Cruikshank 1992. Satellites of Mars: Geologic history. In *Mars* (H. H. Kieffer, B. M. Jakosky, C. W. Snyder and M. S. Matthews, Eds.), pp. 1257–1282. Univ. of Arizona Press, Tucson.

Thomas, P., J. Veverka, D. Simonelli, P. Helfenstein, B. Carcich, M. J. S. Belton, M. E. Davies, and C. Chapman 1994. The shape of Gaspra. *Icarus* **107**, 23–36.

Thomas, P. C., J. Joseph, B. Carcich, J. Veverka, B. E. Clark, J. F. Bell III, A. W. Byrd, R. Chomko, M. Robinson, S. Murchie, L. Prockter, A. Cheng, N. Izenberg, M. Malin, C. Chapman, L. A. McFadden, R. Kirk, M. Gaffey, and P. G. Lucey 2002. Eros: Shape, topography, and slope processes. *Icarus* **155**, 18–37.

Trombka, J., S. Squyres, J. Bruckner, W. Boynton, R. Reedy, T. McCoy, P. Gorenstein, L. Evans, J. Arnold, R. Starr, L. Nittler, M. Murphy, I. Mikheeva, R. McNutt, T. McClanahan, E. McCartney, J. Goldsten, R. Gold, S. Floyd, P. Clark, T. Burbine, J. Bhangoo, S. Bailey, and M. Petaev 2000. The elemental composition of asteroid 433 Eros: Results of the NEAR-Shoemaker X-ray spectrometer. *Science* **289**, 2101–2105.

Veverka, J., M. Noland, C. Sagan, J. Pollack, L. Quam, R. Tucker, B. Eross, T. Duxbury, and W. Green 1974. A Mariner 9 atlas of the moons of Mars. *Icarus* **23**, 206–289.

Veverka, J., P. Thomas, D. Simonelli, M. J. S. Belton, M. Carr, C. Chapman, M. E. Davies, R. Greeley, R. Greenberg, J. Head, K. Klassen, T. V. Johnson, D. Morrison, and G. Neukum 1994. Discovery of grooves on Gaspra. *Icarus* **107**, 72–83.

Veverka, J., P. Thomas, A. Harch, B. Clark, J. F. Bell, B. Carcich, J. Joseph, C. Chapman, W. Merline, M. Robinson, M. Malin, L. A. McFadden, S. Murchie, S. E. Hawkins, R. Farquhar, N. Izenberg, and A. Cheng 1997. NEAR's flyby of 253 Mathilde: Images of a C asteroid. *Science* **278**, 2109–2114.

Veverka, J., M. Robinson, P. Thomas, S. Murchie, J. Bell, N. Izenberg, C. Chapman, A. Harch, M. Bell, B. Carcich, A. Cheng, B. Clark, D. Domingue, D. Dunham, R. Farquhar, M. Gaffey, E. Hawkins, J. Joseph, R. Kirk, H. Li, P. Lucey, M. Malin, P. Martin, L. McFadden, W. Merline, J. Miller, W. Owen, C. Peterson, L. Prockter, J. Warren, D. Wellnitz, B. Williams, and D. Yeomans 2000. NEAR at Eros: Imaging and spectral results. *Science* **289**, 2088–2097.

Wetherill, G. W., and C. R. Chapman 1988. Asteroids and meteorites. In *Meteorites and the Early Solar System* (J. F. Kerridge and M. S. Matthews, Eds.), pp. 35–67. Univ. of Arizona Press, Tuscon.

Wilkison, S., and M. Robinson 2000. Bulk density of ordinary chondrite meteorites and implications for asteroidal internal structure. *Meteor. Planet. Sci.* **35**, 1203–1213.

Wilson, L., K. Keil, and S. J. Love 1999. The internal structures and densities of asteroids. *Meteor. Planet. Sci.* **34**, 479–483.

Yeomans, D., P. Antreasian, J. Barriot, S. Chesley, D. Dunham, R. Farquhar, J. Giorgini, C. Helfrich, A. Konopliv, J. McAdams, J. Miller, W. Owen, D. Scheeres, P. Thomas, J. Veverka, and B. Williams 2000. Radio science results during the NEAR-Shoemaker spacecraft rendezvous with Eros. *Science* **289**, 2085–2088.

Zappala, V., P. Farinella, Z. Knezevic, and P. Paolicchi 1984. Collisional origin of the asteroid families: Mass and velocity distributions. *Icarus* **59**, 261–285.

Zuber, M. T., D. E. Smith, A. F. Cheng, J. B. Garvin, O. Aharonson, T. D. Cole, P. J. Dunn, Y. Guo, F. G. Lemoine, G. A. Neumann, D. D. Rowlands, and M. H. Torrence 2000. The shape of 433 Eros from the NEAR-Shoemaker laser rangefinder. *Science* **289**, 2097–2101.